Nanostructure Development in Wet Amorphous Amylopectin as Revealed by In Situ X-Ray Scattering Methods

R. K. Bayer,* F. J. Baltá-Calleja

Instituto de Estructura de la Materia, CSIC, Serrano 119, 28006 Madrid, Spain

Received 20 September 2005; accepted 21 November 2005
DOI 10.1002/app.23822
Published online in Wiley InterScience (www.interscience.wiley.com).

ABSTRACT: Completely amorphous, transparent bars of amylopectin were prepared by injection molding of pure native semicrystalline samples (Waxy Maize). The formation of a semicrystalline morphology was studied during annealing treatment at various temperatures in a wet atmosphere, using simultaneous WAXS and SAXS. Amylopectin samples crystallized during 20 days in a humid atmosphere at room temperature and subjected to a successive melting process were also studied by X-ray scattering. Results indicate that individual molecules crystallize independently from each other, similar to the case of native amylopectin grains. During the first stages of crystallization, the changes in the SAXS pattern suggest that uncorrelated crystal blocks are formed, which may arrange to lamellae (if a secondary network of double-helix net-points is hydrothermally dissociated). At the beginning of the crystallization process, only few amylopectin molecules (about 10%) are incorporated into the nanostructure. A shell-like structure of semicrystalline layers, comparable to that of a native grain, develops. When crystallization proceeds further, the initially thin shell layers thicken. This causes the amorphous interlayers to be subjected to inner tensions, leading to a decrease in the melt temperature. After a storage time of 20 days in a humid atmosphere, amylopectin reaches a crystallinity level of 54%, only slightly lower than that of the initial native grains. Upon heating the retrograded amylopectin, immediately before complete melting, the long-period shows a value of 15 nm with a crystal thickness, derived from WAXS, of only 4 nm. Such a structure, which has not been reported before, is due to the relaxations of the inner tensions during melting, which lead to a disappearance of inserted interlamellar crystals. J Appl Polym Sci 100: 3832–3839, 2006

Key words: amorphous amylopectine; WAXS; SAXS; crystallization; nanostructure development

INTRODUCTION

It is known that amylopectin (AP), the highly branched component of starch, crystallizes in the form of concentric spherical shells, which may also build the native grain.[1,2] Jenkins et al.[3] discussed this model, considering the shells to be formed by alternating crystalline–amorphous layers. The crystals consist of chain-ends being organized as parallel strands of double helices. The outer chain-ends form bunches, which are coupled by branched zones to a spacer molecule, which is connected to the AP main chain. The high branching density zones are transformed into the amorphous interlayers. This semicrystalline nanostructure, typically predetermined by the chemical structure of the amylopectin molecule, is characterized by a long-period of $L = 9$ nm, which has been measured for a number of botanically different native starches. The thickness of the nanocrystals is ~7 nm, while the amorphous layers are about 2 nm thick. The main chains originate from the center (hilum) of the star-shaped AP molecule, where they are coupled in an unknown manner. They extend radially from the center, thus giving rise to the shell-shaped structure. The spherical shells may also be recognized as growth rings that form during synthesis by enzymes. Within the semicrystalline shells, a shell-shaped amorphous underground is located. If the native grain contains amylose, it is situated in the amorphous underground. According to Ziegler et al.,[1] amylose containing shells are preferentially located in the interior of the grain. The crystallized native grain appears as an asteroid-like branched amylopectin molecule with bunches of outstanding parallel linear chain-ends. The high organization of the native grain can be easily disturbed, for

Correspondence to: R. K. Bayer (rbayer@uni-kassel.de).
**Present address:* R. K. Bayer, Universität Gesamthochschule Kassel, Mönchebergstr.3, D-34125 Kassel, Germany.
Contract grant sponsor: MEC, Spain; contract grant number: FIS2004–01,331.
Contract grant sponsor: Secretaría de Estado de Universidades e Investigación, MEC and the European Social Fund; contract grant number: SAB2003–0131.
Contract grant sponsor: European Community ; contract grant number: HPRI-CT-1999–00,040.
Contract grant sponsor: Deutsche Forschungsgemeinschaft.

example, by a drying process. Donald et al.[4,5] regard the amylopectin as a polymer showing a liquid crystalline structure with mesogenic groups in the side chains. These stiff entities constitute chain-ends, which organize themselves by winding two single helices originating from a branching point into double helices. Branching zones and spacer molecules, as well as the backbone itself, are considered as flexible single-helix starch chain molecules. In the nematic phase, the stiff chain-ends are parallel oriented, without getting a lamellar (smectic) order. This is possible only by an increase in the molecular mobility, for instance, by water penetration. The molecular motion leads to the long-period mentioned earlier. Donald et al.[6] also mention that the AP lamellae may drill, which might reflect a radial fiber-structure[2] particularly being located in the outer zones of the concentric shells.

The length of the outer chain-ends is essential for the crystallization of the amylopectin molecule. Since the crystal lamellae, for reasons of thermodynamic stability, must have a minimum thickness, the outer chains should not be too short. The chain-ends may not be too long, because chain folding may take place. A back folding of a stiff double-helix chain would, however, introduce so much instability that the lamellar crystals might disintegrate. According to Vandeputte et al.[7] and Shi and Seib,[8] amylopectin crystallization is possible only if chain-ends exhibit lengths in the range 12–22 monomers. No crystallization is feasible for chain-ends below and above that critical length region. Accordingly, as pointed out earlier, amylopectin crystals normally have a thickness of ~7 nm corresponding to 16 monomers, just within the aforementioned range. One can therefore assume that if crystallization of AP molecules is observed, chain-ends must exhibit a mean length within this range.

Our own studies[9,10] suggest that the network of starch consists of two components. Up to 120–130°C, one observes a temperature-resistant component only from amylose, which refers to fixed entanglements preformed in the melt (primary component). However, just below 70°C, a secondary component from double-helix network-points is formed.

According to Gidley,[11] the formation of starch gels is characterized by this double-helix network. The secondary network incorporates both amylose and amylopectin, since double-helix bonding may be possible both from single helices of amylose as well as from amylopectin outer chain-ends.[12] Because the initially amorphous injection-moldings investigated here consist of amylopectin alone, a coupling between molecules can occur only through the secondary network.

The structural study of injection-molded starch in relation to the micromechanical properties has been the objective of investigations done in our laboratory.[13,14] In a preceding work, the structural and polymorphic changes of injection-molded starch during heat treatment, in a humid atmosphere, were studied using simultaneous SAXS and WAXS methods.[15] The aim of the present study is to discuss in detail the development of further nanostructural parameters of wet-conditioned amylopectin as a function of heat treatment.

EXPERIMENTAL

Injection-molded bars of amylopectin with a cross section of 4×4 mm^2 were prepared by injection molding.[16,17] One-millimeter thick pieces cut from the bars were placed into a humid atmosphere to observe the retrogradation phenomena. A set of samples was previously prepared as a semicrystalline gel by storing them for 20 days in humid atmosphere. Both sets of samples were subjected to a successive heating program, yielding an increased crystallization on the one hand and a partial melting on other hand.

Evaluations refer to the previously reported SAXS and WAXS data.[15] In the present study, a more detailed evaluation is carried out. In addition to the total degree of crystallinity (X_c), the long-period (L), the size of the coherently diffracting domains (t), and the SAXS invariant (Q), also the degree of crystallinity within the lamellar stacks (X_{cL}), the fraction of lamellar stacks within the spherulite (X_L), the fraction of crystallizing units (X_S), and the thickness of the amorphous (l_a) and crystalline layers (l_c) are discussed.

During the beginning of the crystallization process (primary crystallization), the spherulites do not cover the whole volume of the material. Following Ref. 18, let us call the fraction of spherulites X_S. Large amorphous areas may exist between the lamellar stacks within the spherulite. Les us denote the fraction of the lamellar stacks within the spherulites as X_L. Summarizing the last two points, it can be said that in the case of a not-yet-completed crystallization, lamellar stacks might be inserted within an amorphous matrix, whose fraction is given by $(1 - X_S X_L)$.

The total crystallinity of the system can be written as

$$X_c = X_S X_L X_{C_L} \tag{1}$$

Let us recall that the invariant is determined by integrating the SAXS over all scattering angles:

$$Q = 2\pi / V \int I s^2 ds \tag{2}$$

where I is the SAXS intensity, V is the scattering volume of the sample, and $s = 2 \sin \theta/\lambda$ is the scattering vector. Generally Q is related to the structure of an ideal two-phase model by means of equation

$$Q = x(1 - x)\Delta\rho^2 \tag{3}$$

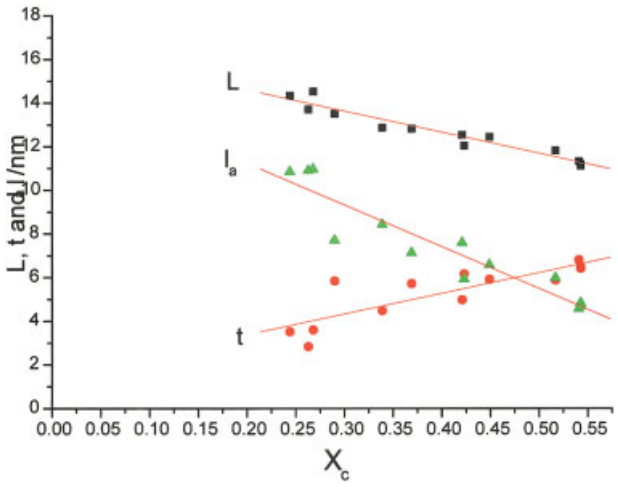

Figure 1 Plot of long-period L, width of the mosaic-blocks t, and amorphous layer thickness $l_a = L - t$ as a function of degree of crystallinity. (20-day retrograded amylopectin in wet atmosphere at room temperature). [Color figure can be viewed in the online issue, which is available at www.interscience.wiley.com.]

x being the volume fraction of one-phase and $\Delta\rho$ the electron density difference between the two-phases. In the case of lamellar stacks from alternating crystalline and amorphous layers, eq. (3) can be written as:

$$Q = X_{cL}(1 - X_{cL})\Delta\rho^2 \tag{4}$$

If there exist purely amorphous regions outside the lamellar stacks, these do not contribute to the integrated SAXS intensity. Equation (4) then transforms to eq. (5), which is generally valid.

$$Q = X_S X_L[X_{c_L}(1 - X_{cL})\Delta\rho^2] \tag{5}$$

Assuming that Wulf's law applies, $l_c \cong \xi t$ ($\xi \sim 1$–2),[19] relating the crystallite size in the chain direction l_c and in the perpendicular direction to it t, one may derive the degree of crystallinity within the lamellar stack as

$$X_{cL} = t/L \tag{6}$$

If one knows X_c and X_{cL}, since the volume of the sample does not appreciably vary with the temperature and time of the experiment, from eqs. (1) and (2), one may calculate the parameter $\Delta\rho^2$, which is proportional to $\Delta\rho^2$ and differing by a factor V.

RESULTS AND DISCUSSION

Highly crystallized potato starch gel

The initial amylopectin sample was obtained by crystallization of an amorphous structure subjected to a 20-day treatment in a humid atmosphere at room temperature. A crystallinity of $X_c \sim 54\%$ is attained by this way. In comparison, $X_c = 58\%$ was measured for the native Waxy Maize before injection molding. This implies a considerable recovery of the native crystalline structure before injection molding. The crystallinity changes were induced through a partial melting. Figure 1 shows the variation of the nanostructural parameters L and t as a function of the total degree of crystallinity X_c.

One striking result that attracts attention, which is not observed for other starch samples (i.e., potato starch[20]) or other semicrystalline synthetic polymers, is that t increases with X_c and that t decreases when X_c is reduced.

Usually, when crystallization starts, (i.e., at low X_c) only thicker crystals are formed. In the case of partial melting, for low X_c values, only thicker crystals are left. When X_c increases, thinner crystals originate by insertion between the already existing lamellae, reducing L as well as the average crystal-thickness l_c (simultaneously the width t of the mosaic blocks).

In case of amylopectin, L decreases with X_c, as expected, while t exhibits an increase with X_c unexpectedly. The plot of X_{cL} as a function of X_c (Fig. 2) leads us to the peculiarities of the crystallization of amylopectin.

The experimental results are well described by the relationship

$$X_{cL} = X_c \tag{7}$$

From eqs. (1) and (7), it follows $X_S X_L = 1$. See also Figure 2. By the combination of eqs. (1), (6), and (7) one obtains:

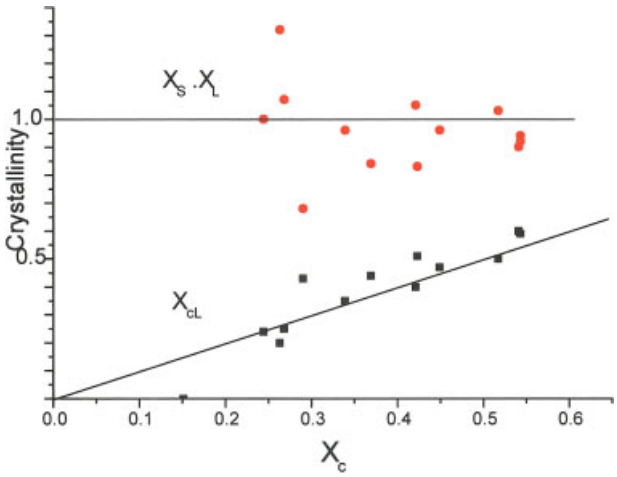

Figure 2 Plot of linear crystallinity $X_{cL} = t/L$ and fraction $X_S X_L$ as a function of total degree of crystallinity (20-day retrograded amylopectin in humid atmosphere, later partially melted). [Color figure can be viewed in the online issue, which is available at www.interscience.wiley.com.]

$$X_S X_L = X_c\, L/t \tag{8}$$

The $X_S X_L$ fraction may vary substantially when X_c and t/L are small. This gives rise to the fluctuations of $X_S X_L$ observed in Figure 2 for low X_c values. The fact that $X_S X_L = 1$ even for $X_c < 0.5$ is an uncommon result too. In case of other polymers, one observes for $X_c < 0.5$ the loss of the percolation of the crystals ($X_S X_L < 1$), which then are unconnected in an amorphous matrix. Furthermore, in our case, X_{cL} values smaller than 0.5 are observed (see Fig. 2). At least, shortly before complete melting (small X_c values), crystals should exhibit a high perfection, that is, a high value of X_{cL}. In the present case, we measure for $X_c = 0.25$ just a similar low value of X_{cL}. Since X_S as well as X_L may vary from 0 to 1, from the condition $X_S X_L = 1$, it follows that $X_S = 1$ and, in addition, $X_L = 1$. The requirement $X_L = 1$ implies that there are no lateral amorphous zones between the lamellar stacks. This is already a known result for the structure of the native amylopectin grain.

A crystallized amylopectin molecule shows a shell-like crystalline lamellae nanostructure.[1–3] Nanolayered crystal-blocks, which are arranged into a spherical lamellar shell, only have crystals as nearest neighbors. A stack of lamellae, composed from concentric spherical shells of different diameters, does not exhibit the ends of lamellae. Hence, an amorphous neighborhood directly beside the lamellae of the stack is excluded by the shell-like conformation of the lamellae. No more lateral growth is allowed to the spherical shaped lamella. Apparently, amylopectin recrystallizes from the amorphous state, induced by water penetration, into a crystal-morphology similar to that of the native grain. This is not surprising, if one takes into account that the crystal morphology of amylopectin is strongly related to the branched structure of the amylopectin molecule.

The other result $X_S = 1$, at least for $X_c = 0.54$ may be well understood. It is not expected that at high crystallinities any amylopectin molecule remains amorphous. The result $X_S = 1$, even for small X_c (short before the melting up), means that all amylopectin molecules remained crystalline; however, its crystal shells ($X_L = 1$) become very thin ($t = l_c = 4$ nm) and are located at a wide distance apart from each other ($L = 15$ nm). The extrapolation $L(X_c)$ for $X_c \to 0$ (Fig. 1) reaches even 16 nm. This state of amylopectine crystallization was unknown until now. The standard structure of amylopectin molecules in native, crystallized condition is given by $L = 9$ nm and $X_{cL} = 0.5$. Because of the obstacles (such as branching) to crystallization as quoted earlier, a growing shell crystal may be thermodynamically less stable than an initial thin layer. The melt entropy increases, which makes the melting point to decrease during the progress of crystallization in spite of the increment of thickness.

The model of Waigh[21] illustrates such a growth of crystal lamellae of the amylopectin molecule by a lon-

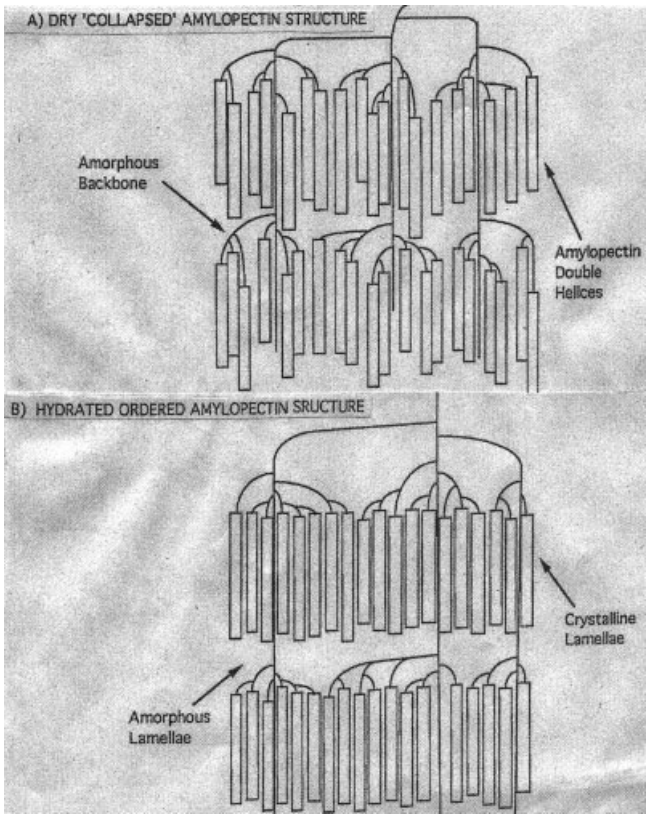

Figure 3 Model of Waigh.[21]

gitudinal arrangement of the double helices and a simultaneous tension of the branched amorphous layers (increase of the melt entropy, Fig. 3).

To obtain a parallel structure of chain-ends of the bundles of the grape-like structure of the amylopectin, an entropically unfavorable order of the branches, which lead to the outer bundles, is required. This feature of the amylopectin crystallization is related to the inner tensions of the amorphous zones. The simultaneous decrease of the long-period with crystallinity (Fig. 1) could be explained by insertion of new, probably more stressed lamellae into the interspaces of the newly formed shell crystals. On the other hand, the insertion model can explain the successive melting of a well-retrograded amylopectin. Firstly, the highly stressed interlamellae become so much affected that after a decrease of thickness they finally break into smaller entities (Fig. 4). The remaining fragments of the interlamellae are not so well coordinated that they do not contribute any longer to the long-period (L increases), while they still contribute to the decreasing mean value of t.

The shell model, supplemented by the hindrance to crystallization due to the inner tensions within the amorphous layers, could explain the thermodynamically paradoxical behavior of the system. On one hand, the thick stressed crystal blocks start melting while L increases, and on the other, at the end of the melting process, only few thin stress-free spherical shells with low X_{cL} crystal perfection remain.

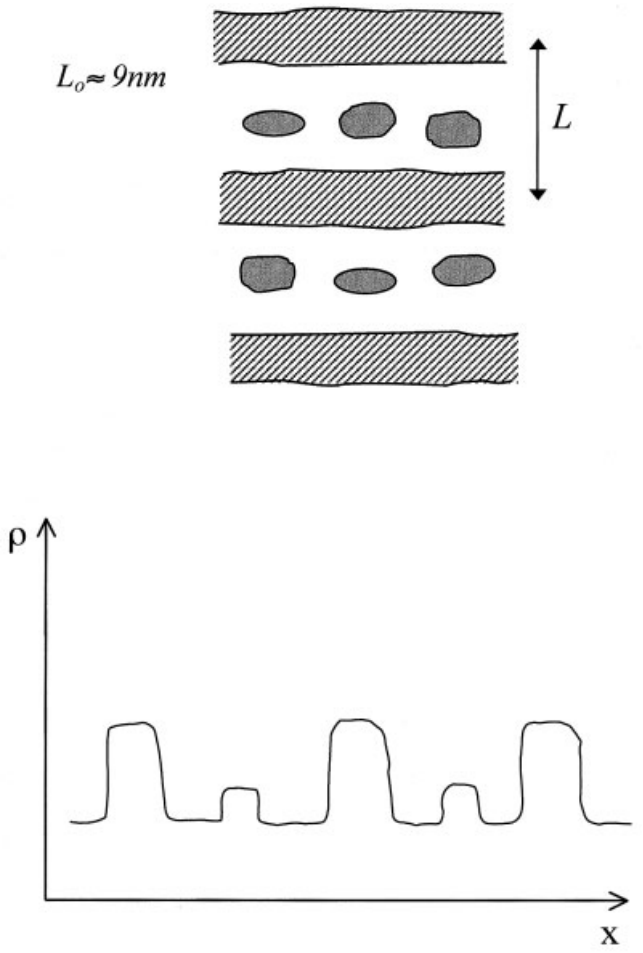

Figure 4 Scheme of long-period increase after breaking of lamellae (top). Electron density profile (bottom).

The spherical shell model of crystallized amylopectin suggests that $X_S X_L = 1$; this yields $X_{cL} = X_c$. Because X_{cL} is defined as l_c/L [see eq. (6)], this holds for any state of crystallization of amylopectin; that is, $l_c/L = X_c$. Since from Figure 6 one derives that $t/L = X_c$, therefore, for amylopectin it follows: $t = l_c$.

Figure 5 illustrates the melting process as a function of the time and temperature program applied. One sees that $X_S X_L = 1$ holds up to 94°C, while X_c reduces to 25%. The morphology has already been described as wide distanced ($L = 15$ nm) thin shells ($t = 4$ nm, Fig. 6). Because no more long-period is observed at 113°C, this structure disrupts to uncoordinated crystal blocks ($X_c \sim 20\%$). $X_S X_L$ rapidly falls to zero, and the crystalline rests are not very resistant against melting, as expressed by the accelerated decrease of X_c (Fig. 5). Figure 7 indicates that the quantity $\Delta\rho'^2$ as calculated from the experimentally determined Q', X_c, t, and L values (eq. (9)), depending on X_c.

$$\Delta\rho'^2 = Q'/X_c \cdot (1 - X_{cL}) \qquad (9)$$

For $X_c = 20\%$, $\Delta\rho'^2$ approaches zero. This decrease starts in the 75°C temperature interval (Fig. 8). All

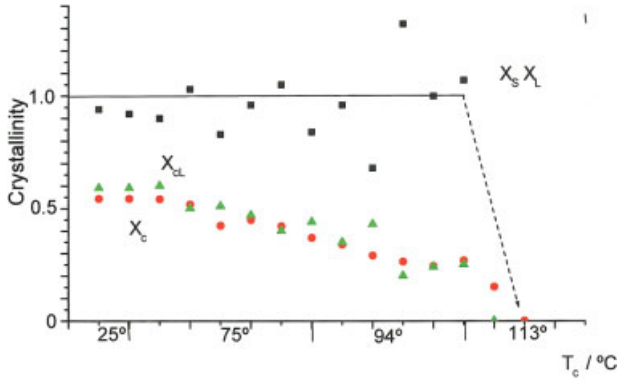

Figure 5 Variation of total crystallinity X_c, linear crystallinity X_{cL}, and the fraction $X_S X_L$ as a function of temperature and time. [Color figure can be viewed in the online issue, which is available at www.interscience.wiley.com.]

Figures (5, 6, and 8) above the third point (first of the 75°C temperature level) show a clear change of the course of the measured curves. Following ref. 9 the secondary network of double-helix net-points is molten at that temperature. Figure 8 shows that $\Delta\rho'^2 \sim (\rho_c - \rho_a)^2$ starts to decrease when the secondary network melts. This explains the unexpected result that at $X_c = 20\%$ (extrapolated in Fig. 7) the electron density difference tends to zero. When the secondary network melts, the crystalline gel begins to exude water. Because the free water is stored in the amorphous zones, ρ_a must now increase and approach the value of ρ_c, that is, $\Delta\rho'^2$ decreases as observed in Figure 8. No change of ρ_c is expected, because t during the strong $\Delta\rho'^2$ decrease at 75°C is maintained above 5 nm (Fig. 6), that is, 12 monomers, which is in between the stability range of AP crystals of 12–22.[7]

The successive melting process is, hence, superimposed by an exudation of water from the gel from 75°C

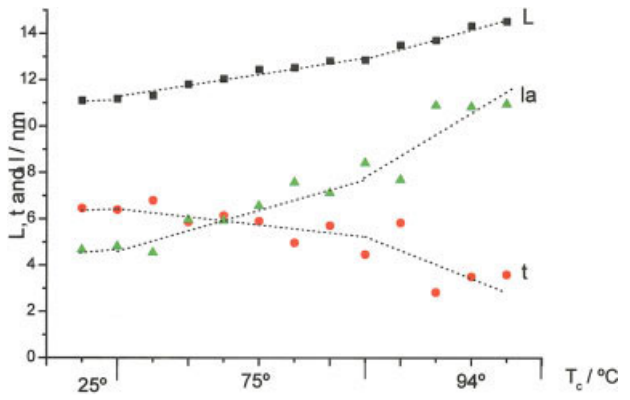

Figure 6 Variation of long-period L, mosaic-block size t, and thickness of the amorphous layer l_a, with temperature and time for 20-day retrograded amylopectin (see text). [Color figure can be viewed in the online issue, which is available at www.interscience.wiley.com.]

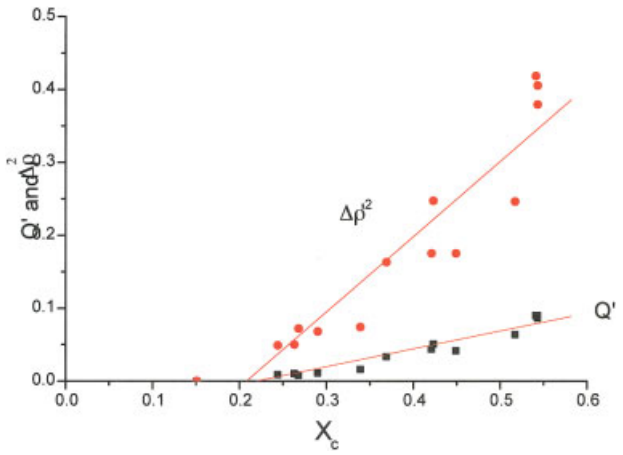

Figure 7 Invariant from SAXS, Q' and $\Delta\rho'^2$ from eq. (5) as a function of degree of crystallinity (20-day retrograded amylopectin in humid atmosphere). [Color figure can be viewed in the online issue, which is available at www.interscience.wiley.com.]

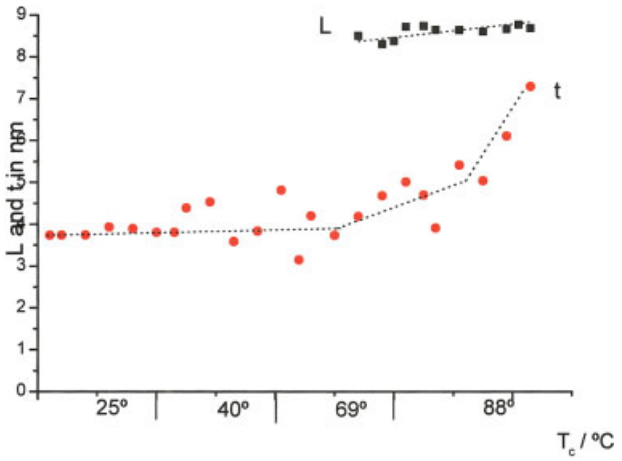

Figure 9 Plot of long-period L and lateral mosaic-block size t, during a stepwise heating (each temperature is held 10 min). Start of the retrogradation of amorphous amylopectin in a humid atmosphere. [Color figure can be viewed in the online issue, which is available at www.interscience.wiley.com.]

onwards. This drying process, however, does not prevent the complete melting of the concentrated gel at 113°C. The crystalline residues of the original shell structure (X_c = 20%) are embedded in a stiff amorphous matrix of nearly the same density as the crystals.

Early state of retrogradation of air-dry amorphous ap in moist atmosphere

The beginning of retrogradation of amorphous amylopectin in saturated humid atmosphere supports well the main results discussed in the previous section: with increasing temperature of crystallization the value of t indeed increases (Figs. 9, 10).

Figure 9 also shows that crystallites with a size of 4 nm (nearly 10 monomers) are created immediately after the insertion of the sample into the moist atmosphere. The crystals do not form regular stacks as evidenced by the absence of a SAXS long-period.

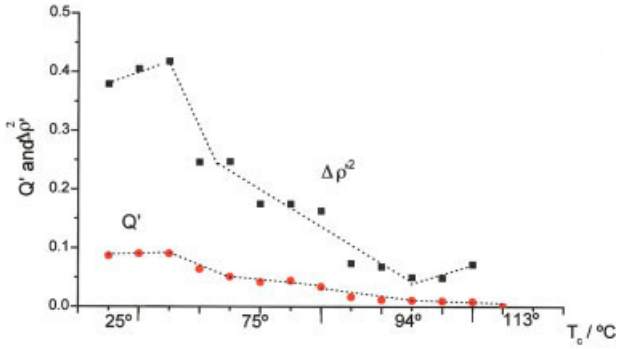

Figure 8 Variation of the invariant Q' of SAXS and $\Delta\rho'^2$ as a function of temperature and time. [Color figure can be viewed in the online issue, which is available at www.interscience.wiley.com.]

The arrangement of these crystal-blocks into lamellar stacks does not take place below $T_c \sim 69$°C. At lower temperatures, a secondary double-helix network[9,10] of the still dry amorphous injection-molding prevents the first crystals to build up an arrangement of lamellae. The secondary network provides, in addition, the molecular cohesion within the initially amorphous system. Because of the absence of a primary network from entanglements, mechanical properties however remain poor (brittle fracture at low deformations). Just after the thermal disintegration of the secondary network (69°C), shell-shaped lamellae

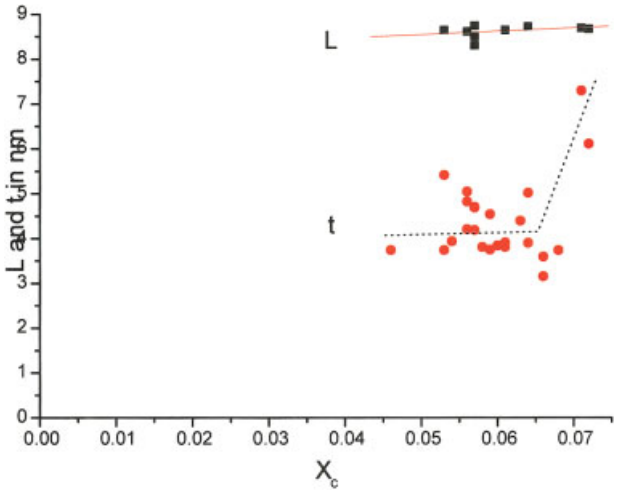

Figure 10 Plot of long-period L and lateral mosaic block size t as a function of total degree of crystallinity. Start of the retrogradation of amorphous amylopectin. [Color figure can be viewed in the online issue, which is available at www.interscience.wiley.com.]

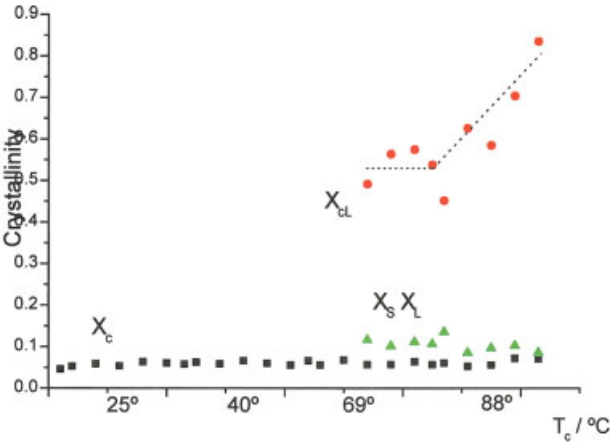

Figure 11 Total degree of crystallinity X_c, linear crystallinity X_{cL}, and fraction $X_S X_L$ with increasing stepwise temperature. Early state of retrogradation of amorphous amylopectin. [Color figure can be viewed in the online issue, which is available at www.interscience.wiley.com.]

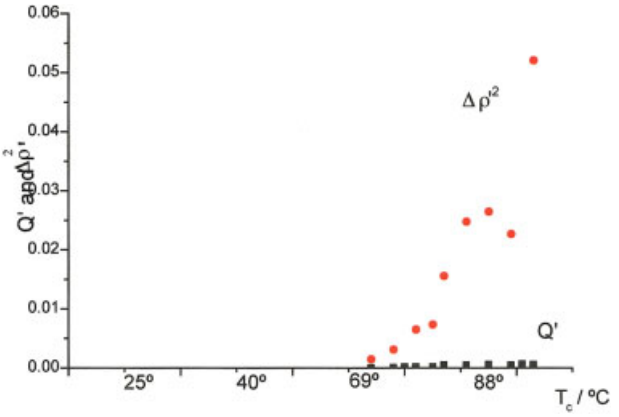

Figure 13 Development of Q' and $\Delta\rho'^2$ during the early stages of retrogradation of amorphous amylopectin. [Color figure can be viewed in the online issue, which is available at www.interscience.wiley.com.]

form immediately, as Figure 9 clearly shows that t rises quickly from 4 to 7.5 nm, while L remains constant. Because of the lack of entanglements[9,10,22] in the amorphous amylopectin, there are no obstacles that could prevent the described crystallization of individual molecules.

During the stepwise temperature increase, the total crystallinity does not increase further beyond $X_c = 7\%$ (Figs. 11 and 12). If the same temperature program is applied to amorphous injection-moldings of potato starch, then retrogradation leads to $X_c = 30\%$. In this case, a periodic structure is obtained much earlier.[20]

The increase of t and X_{cL} through the increase of X_c (see Figs. 10 and 12) supports the concept of the same spherical shell-like crystallization of the amylopectin molecules as discussed in the preceding section. From

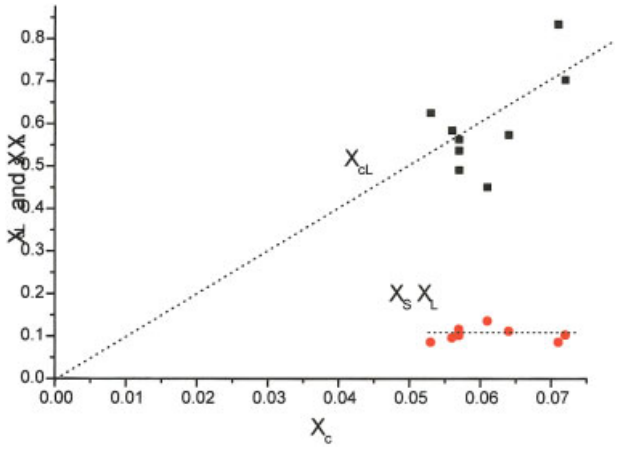

Figure 12 Variation of linear crystallinity X_{cL} and the fraction $X_S X_L$ as a function of total degree of crystallinity X_c (data from Fig. 11). [Color figure can be viewed in the online issue, which is available at www.interscience.wiley.com.]

the values of $X_S X_L$ (Fig. 12), one would expect that not more than 10% of all amylopectin molecules crystallize in concentric shell-shaped lamellae. These amylopectin molecules are especially able to crystallize with X_{cL} values reaching up to 0.8 when X_c increases (see also Fig. 2). Possibly, the first crystallizing amylopectin molecules contain longer chains in the ends, forming bundles similar to Figure 3. According to Ref. 12, this would facilitate crystallization. A lower density of the branched zones could reduce the inner stresses in the amorphous zones, and thus, reduce resistance to crystallization. The slope of X_{cL} (X_c) in Figure 12 is about a factor $1/X_S X_L$ steeper than in Figure 2 because only 10% of the molecules are involved in the early stages of crystallization. If the value of X_c is referred only to the semicrystalline zones ($X_S X_L$), the straight line of Figure 12 would coincide with the X_{cL} variation of Figure 2, also characteristic for the shell model. If amylopectin crystallizes, the whole large molecule (up to 100 μm diameter) should crystallize. Because of the radial symmetric structure, only the arrangement in a semicrystalline shell-like spherical structure is possible.

The long-period does not change very much ($L \approx 9$ nm; see Figs. 9 and 10). This value is rather low in comparison with those obtained during partial melting of a well-crystallized amylopectin (11–15 nm; see Figs. 1 and 4). On the other hand, it corresponds quite well to the long-period of most of native starch substances containing amylopectin. This characteristic value has been explained by the chemical structure of the amylopectin molecule (see Introduction).

Figure 13 shows a strong increase in $\Delta\rho'2$ in the temperature interval of 88°C. This can be ascribed to a strong increase of X_{cL} (Fig. 11) and an increment of t (Fig. 9) parallel to an arrangement of crystal blocks to a periodic crystalline lamella stack (existence of L) (see Fig. 9). Wide angle X-ray diffraction patterns indicate that the pene-

tration of water into the sample can be identified. Thus, the crystals at low temperatures do not give rise to crystalline X-ray scattering. They are only 4 nm thick, corresponding to 9 monomers, that is, below the stability range of 12–22 monomers for amylopectin crystals.[7] Hence, these crystals may be considered as precursors of a emerging crystalline structure embedded into an amorphous amylopectin matrix.

It is remarkable that $L = 9$ nm is not observed near the end of the melting process of the 20-day retrograded amylopectin (see Fig. 6). The difference between these two crucial structures ($L = 9$ nm and $L = 15$ nm) may be due to different types of amylopectin molecules. Let us assume that the 15-nm long-period structure refer to the densely ramified amylopectin molecules. Inner stresses in the well-crystallized state should then increase. Particularly, the later formed interlamellae will be strongly stressed. The inner stresses should lead to molecular displacements of the uncrystallized single-helix chains, including the backbone. This should contribute to a plastic deformation favorable for the formation of the crystals. During heating, a stress relaxation could melt first interlamellae, and the remaining plastic deformation would give rise to a continued existence of farther away lamellar crystals ($L = 15$ nm). The remaining thin crystalline shells are a remainder of a foregoing highly crystalline structure containing high inner stresses.

CONCLUSIONS

1. When amorphous injection-molded amylopectin starch is annealed in a humid atmosphere at room temperature, a total crystallinity of 54% is reached. This degree of crystallization is close to that of the native grain. From the study of the successive melting behavior of that structure, it is suggested that nanolayered crystals as well as amorphous interlamellar regions similar to those in native grain may exist as concentric shells.
2. Results indicate that this holds for all the amylopectine molecules of the material. Therefore, no crystalline superstructure, which incorporates more than one amylopectin molecule, occurs. After annealing, grains similar to those before injection molding are formed again. During the growth of crystals, the amorphous interlamellar regions are stressed, leading to a decrease of the melting point.
3. The cohesion of the amorphous material is given by a secondary network, which joins molecules to each other through double-helix bonding. Owing to the absence of an amylose primary network, the mechanical properties are, however, rather poor. Small deformations give rise to a brittle fracture. When humidity diffuses into the amorphous molding, the first isolated nanocrystals are immediately formed. After melting the secondary network at 70°C, an X-ray long-period from a shell-like nanostructure is built up, indicating the presence of crystal stacks.
4. The spherical semicrystalline shell nanostructure, which is formed after a 20-day annealing process in a humid atmosphere and subsequent partial melting ($L = 15$ nm), is different from that obtained when water starts penetrating the initially amorphous amylopectin starch ($L = 9$ nm). This can be correlated to a partial melting of crystal shells located between strongly stressed amorphous interlamellar regions.

The SAXS and WAXS data discussed in this work were derived from measurements carried out at HASYLAB, DESY, Hamburg, under project II-04–029 EC. The Arburg Company in Lossburg, Germany is thanked for kind supply of the injection-molding machine used.

References

1. Ziegler, G. R.; Creek, J. A.; Runt, J. Biomacromolecules 2005, 6, 1547.
2. Lemke, H.; Burghammer, M.; Flot, D.; Rossle, M.; Riekel, C. Biomacromolecules 2004, 5, 1316.
3. Jenkins, P. J.; Cameron, R. E.; Donald, A. M.; Bras, W.; Derbyshire, G. E.; Mant, G. R.; Ryan, A. J. J Polym Sci Part B: Polym Phys 1994, 32, 1579.
4. Waigh, T. A.; Perry, P.; Riekel, C.; Gidley, M. J.; Donald, A. M. Macromolecules 1998, 31, 7980.
5. Waigh, T. A.; Gidley, M. J.; Komanshek, B. U.; Donald, A. M. Carbohydr Res 2000, 328, 165.
6. Waigh, T. A.; Kato, K. L.; Donald, A. M.; Gidley, M. J.; Clarke, C. J.; Riekel, C. Starch/Stärke 2000, 52, 450.
7. Vandeputte, G. E.; Vermeylen, R.; Geeroms, J.; Delcour, J. A. J Cereal Sci 2003, 38, 1.
8. Shi, Y. C.; Seib, P. A. Carbohydr Polym 1995, 26, 141.
9. Bayer, R. K.; Cagiao, M. E.; Baltá Calleja, F. J. J Appl Polym Sci, to appear.
10. Bayer, R. J.; Baltá Calleja, F. J. J Macromol Sci Phys 2005, 44, 471.
11. Gidley, M. J. Macromolecules 1989, 22, 351.
12. Klucinec, J. D.; Thompson, D. B. Cereal Chem 2002, 79, 24.
13. Flores, A.; Bayer, R. K.; Krawietz, K.; Baltá Calleja, F. J. J Macromol Sci Phys 2000, 39, 749.
14. Ania, F.; Dunkel, M.; Bayer, R. K.; Baltá Calleja, F. J. J Appl Polym Sci 2002, 85, 1246.
15. Cagiao, M. E.; Bayer, R. K.; Rueda, D. R.; Baltá Calleja, F. J. J Appl Polym Sci 2003, 88, 17.
16. Bayer, R. K.; Zachmann, H. G.; Baltá Calleja, F. J.; Umbach, H. Polym Eng Sci 1989, 29, 188.
17. Lopez Cabarcos, E.; Zachmann, H. G.; Bayer, R. K.; Baltá Calleja, F. J. Polym Eng Sci 1989, 29, 193.
18. Santa Cruz, C.; Stribeck, N.; Zachmann, H. G.; Baltá Calleja, F. J. Macromolecules 1991, 24, 5980.
19. Hosemann, R.; Baltá Calleja, F. J. Polymer 1979, 20, 1091.
20. Bayer, R. K.; Baltá Calleja, F. J. Int J Polym Mater, to appear.
21. Waigh, T. A.; Hopkinson, I.; Donald, A. M.; Butler, M. F.; Heidelbach, F.; Riekel, C. Macromolecules 1997, 30, 3813.
22. Bayer, R. K.; Dietrich, F.; Lindemann, S.; Ania, F. Instituto de Estructura de la Materia, unpublished results.